Available online at www.sciencedirect.com
ScienceDirect
Polymer 47 (2006) 8575–8582
polymer
www.elsevier.com/locate/polymer

# Effect of spreading solvents on Langmuir monolayers and Langmuir–Blodgett films of PS-*b*-P2VP

Gangyao Wen [a,b,*], Bonghoon Chung [a], Taihyun Chang [a,**]

[a] *Department of Chemistry and Center for Integrated Molecular Systems, Pohang University of Science and Technology, Pohang 790-784, Republic of Korea*

[b] *Department of Polymer Materials and Engineering, College of Materials Science and Engineering, Harbin University of Science and Technology, Harbin 150040, PR China*

Received 23 August 2006; received in revised form 7 October 2006; accepted 22 October 2006
Available online 9 November 2006

**Abstract**

Langmuir monolayers of polystyrene-*block*-poly(2-vinylpyridine) (PS-*b*-P2VP) diblock copolymers (with the same PS block length and different P2VP block lengths) formed at the air/water interface were characterized with the Langmuir film balance technique. Nonselective and selective solvents were used to spread the samples on the water surface and the spreading solvents showed large effect on the surface pressure–molecular area isotherms. The corresponding Langmuir–Blodgett (LB) films of the samples were characterized with atomic force microscopy. The LB films transferred from the Langmuir monolayers spread with a nonselective solvent only exhibited isolated circular micelles, while those with a selective solvent exhibited quite different morphologies including planar structure, rodlike structure, circular micelles, and labyrinth pattern. As far as we know, the labyrinth pattern appears in the LB films for the first time.


*Keywords:* LB film; Block copolymer; Spreading solvent

## 1. Introduction

Due to the excellent self-assembled ability, the microdomain structure of block copolymers has been extensively studied in recent years [1–12]. It is well known that amphiphilic block copolymers can usually form the aggregates at the air/water interface [13–35]. The aggregation morphology can be affected by many factors such as nature of the core-forming and corona-forming blocks, composition of the copolymer, nature of the spreading solvent, and condition of the subphase, etc. There are three mechanisms proposed to describe the aggregation phenomenon at the air/water interface: spontaneous surface aggregation [19], compression induced surface aggregation [28,29], and simple deposition of the micelles formed in the spreading solution [30]. Usually, nonselective solvents are used to study the aggregation behavior of block copolymers at the air/water interface so that the block copolymers are in individual chains before spreading. In this paper, on the contrary, we are interested in using a selective solvent to study the aggregation behavior of diblock copolymers at the air/water interface, and we hope we can find some new aggregation morphologies of LB films and do some contributions to the aggregation mechanisms. As we know, solution micelles will exist when a diblock copolymer is dissolved in a selective solvent and the concentration is above the critical micelle concentration (cmc) [36–44]. If the corona-forming block of the solution micelles is attractive to water then the surface aggregation behavior maybe a simple deposition of the micelles formed in the spreading solution. If the core-forming block of the solution micelles is attractive to water, on the other hand, then the block

* Corresponding author. Present address: Department of Polymer Materials and Engineering, College of Materials Science and Engineering, Harbin University of Science and Technology, Harbin 150040, PR China. Tel.: +86 451 8639 2590; fax: +86 451 8639 2522.
** Corresponding author. Tel.: +82 54 279 2109; fax: +82 54 279 3399.
*E-mail addresses:* gywen@hrbust.edu.cn (G. Wen), tc@postech.edu (T. Chang).

0032-3861/$ - see front matter © 2006 Elsevier Ltd. All rights reserved.
doi:10.1016/j.polymer.2006.10.025

would tend to stretch on the water surface but the aggregates retained from the spreading solution would hinder the stretch.

In this work, nonselective and selective solvents were used to spread the Langmuir monolayers of polystyrene-*block*-poly(2-vinylpyridine) (PS-*b*-P2VP) at the air/water interface. The monolayers and the corresponding Langmuir–Blodgett (LB) films were, respectively, characterized with the Langmuir film balance technique and atomic force microscopy (AFM). Temperature effect on the surface pressure–molecular area ($\pi$–$A$) isotherms of the monolayers was also considered. Moreover, dynamic light scattering was performed to obtain the cmc of PS-*b*-P2VP in the selective solvent. The spreading solvents in our system showed large effect on the isotherms of the Langmuir monolayers and on the morphologies of the LB films. We notice that Cox et al. [19] showed that the surface aggregation of another system polystyrene-*block*-poly(ethylene oxide) (PS-*b*-PEO) is a spontaneous process which is neither compression nor spreading solvent dependent [there is no difference in the morphology of the LB films of $PS_{140}$-*b*-$PEO_{80}$ spread with a nonselective spreading solvent (chloroform) and a selective spreading solvent (toluene)]. For PS-*b*-PEO (with less than 7 wt% PEO), however, it has been reported by Baker et al. that the thin film morphology depends on the concentration of spreading solution in the nonselective solvent (chloroform) and three types of features are observed in various proportions: dots (circular aggregates), spaghetti (rodlike aggregates), and continents (planar aggregates) [35]. By the way, Zhu et al. have also observed the above three morphologies in the LB films of polystyrene-*b*-poly(decylated vinylpyridinium iodide) by changing the block polyelectrolyte composition [16,17]. Of course, the above rodlike and planar aggregates are quite different from what we observed in our system (will be mentioned later). In our opinion, the morphology of the LB films of a block copolymer with a very short hydrophilic block is more likely to be affected by the spreading solvent.

## 2. Experimental section

### 2.1. Materials and solvents

Three kinds of PS-*b*-P2VP diblock copolymers with the same PS block length and different P2VP block lengths were previously synthesized in our research group by sequential anionic polymerization. The number-average molecular weights ($M_n$) of PS and P2VP blocks in the three copolymers were, respectively, 28K/11K, 28K/28K, and 28K/59K and the polydispersity indexes of the copolymers were 1.08, 1.05, and 1.05, respectively. According to the $M_n$ of P2VP block, the samples were coded as SVP11, SVP28, and SVP59, respectively. Three kinds of nonselective solvents (good solvent for both PS and P2VP blocks) $CHCl_3$ (Mallinckrodt, HPLC grade), $C_6H_6$ (Janssen, Special grade), and $CH_2Cl_2$ (Duksan, HPLC grade) and a selective solvent (good solvent for PS block but poor solvent for P2VP block) $CCl_4$ (Aldrich, Spectroscopic grade) were used to spread the Langmuir monolayers of PS-*b*-P2VP.

### 2.2. Dynamic light scattering

In order to determine the cmc and the size of the micelles of PS-*b*-P2VP in the selective solvent $CCl_4$, dynamic light scattering was performed at various concentrations. The light scattering instrument was equipped with a Brookhaven goniometer, a photon correlation spectroscopy (Malvern 4700 series), and an argon ion laser (with a wavelength of 514.5 nm). All measurements were made at 25 °C and scattered light was collected at a fixed angle of 90°. The scattering intensity and correlation functions were recorded simultaneously. From the first moment of the correlation function, the translational diffusion coefficient was calculated, which in turn yielded the hydrodynamic radius of the aggregates in solution via the Stokes–Einstein relation.

### 2.3. Isotherm experiments

The $\pi$–$A$ isotherms of the PS-*b*-P2VP monolayers were characterized with a Langmuir film balance apparatus (KSV minitrough, Finland) with an effective film area of 240 × 75 $mm^2$. The water (resistivity of 18.2 MΩ cm) used for the isotherm experiment was purified and deionized with a water purification system (Pure Power II, Human, Korea) equipped with an organic removal cartridge. A platinum Wilhelmy plate was used as the surface pressure sensor. The measurements were performed at 25 °C (unless otherwise specified) by using a refrigerated bath circulator (RBC-10, Jeio Tech, Korea). The moving speed of the barriers was 5 mm/min. According to the evaporation rate, 15 min (for $CHCl_3$ and $CH_2Cl_2$) and 20 min (for $C_6H_6$ and $CCl_4$) were allowed for the evaporation of the spreading solvents before the compression initiated. The concentration of the spreading solutions was 0.50 mg/ml. All the isotherms were run at least two or three times with good reproducibility.

The condition in the hysteresis experiment (compression–expansion cycles) was similar to that in the isotherm experiment. Moreover, when the surface pressure reached a maximum value, the barriers were stopped and kept for 30 s to allow the monolayer to relax. After the expansion was completed, the barriers were kept for 15 min and then the procedure was repeated using progressively higher maximum pressures.

### 2.4. LB films and AFM measurements

KSV minitrough was also used to deposit the LB films onto the silicon wafers (treated with a modified RCA cleaning procedure [45]) at the surface pressures of 2 and 7.5 mN/m. During the deposition, the substrate was dipped into the water (before the spread of the solution) and withdrawn vertically through the monolayer at the speed of 3 mm/min. The LB films were characterized with a tapping mode AFM (Nanoscope IIIa, Digital Instruments) at room temperature. The 10 μm scanner and the etched silicon probe were used. The scan area and speed during the measurements were usually 2 μm × 2 μm and about 0.8–1.0 Hz, respectively. The AFM height images (1 μm × 1 μm) shown here were zoomed from the large ones.

Table 1
Hydrodynamic radius ($R_h$) of the micelles of SVP28 in $CCl_4$ at various concentrations ($c$)

| $c$ (mg/ml) | 0.01 | 0.015 | 0.02 | 0.03 | 0.05 | 0.10 |
|---|---|---|---|---|---|---|
| $R_h$ (nm) | 0 | 0 | 12.0 | 22.0 | 24.8 | 25.0 |

## 3. Results and discussion

### 3.1. Dynamic light scattering

Prior to the study of the Langmuir monolayers, it was necessary to know the properties of PS-*b*-P2VP copolymers in the spreading solvents. In this work, dynamic light scattering was performed to determine the cmc of SVP28 in the selective solvent $CCl_4$. The hydrodynamic radius ($R_h$) of the micelles was calculated by using the Stokes–Einstein relation $R_h = k_B T/6\pi\eta D$, where $k_B$ is the Boltzmann constant, $T$ is the absolute temperature, $\eta$ is the solvent viscosity, and $D$ is the diffusion coefficient. Table 1 lists the $R_h$ of the micelles of SVP28 in $CCl_4$ at various concentrations (up to 0.10 mg/ml). From Table 1, it can be seen that the radii of the micelles rise sharply (from 0 to 12.0 nm) at a concentration of about 0.02 mg/ml, which we identify as the cmc of SVP28 in $CCl_4$. In our $\pi$–$A$ isotherm experiments, the concentration of the spreading solutions was 0.50 mg/ml, which was quite above the cmc of SVP28 in $CCl_4$. Thus, the solution micelles were believed to exist in our spreading solutions of $CCl_4$.

### 3.2. P2VP block length effect on isotherms

Spreading solvents $CHCl_3$ (nonselective) and $CCl_4$ (selective for PS) were used to study the effect of different P2VP block lengths on the isotherms of PS-*b*-P2VP. Fig. 1 shows the $\pi$–$A$ isotherms of SVP11, SVP28, and SVP59 monolayers spread with $CHCl_3$ and $CCl_4$ at 25 °C. From Fig. 1, it can be seen that obvious plateau transition regions exist in the isotherms of SVP28 and SVP59 monolayers spread with

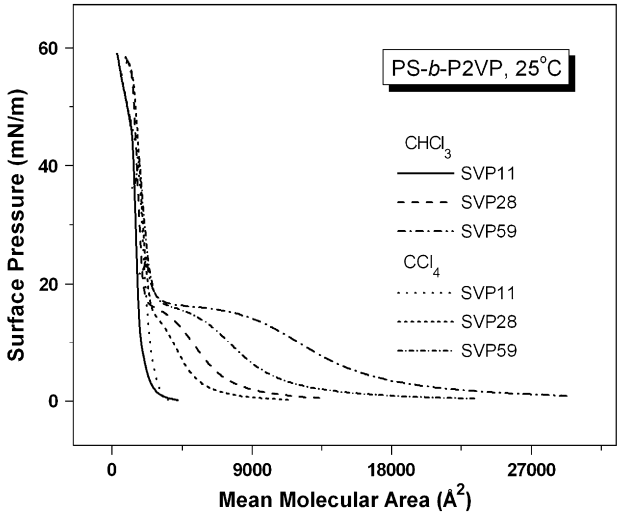


Fig. 1. $\pi$–$A$ isotherms of SVP11, SVP28, and SVP59 monolayers spread with $CHCl_3$ and $CCl_4$ at 25 °C.

Table 2
Some important isotherm parameters for the samples

| Solvent | $CHCl_3$ | | | $CCl_4$ | | |
|---|---|---|---|---|---|---|
| Sample | SVP11 | SVP28 | SVP59 | SVP11 | SVP28 | SVP59 |
| $A_1$ (Å$^2$) | | 4145 | 8636 | | 3466 | 5809 |
| $A_2$ (Å$^2$) | | 2010 | 2732 | | 2395 | 2615 |
| $A_1 - A_2$ (Å$^2$) | | 2135 | 5904 | | 1071 | 3194 |
| $\pi_1$ (mN/m) | | 13.7 | 15.1 | | 12.3 | 14.3 |
| $\pi_2$ (mN/m) | | 17.4 | 16.9 | | 15.9 | 17.2 |
| $\pi_2 - \pi_1$ (mN/m) | | 3.7 | 1.8 | | 3.6 | 2.9 |
| $A_{on}$ (Å$^2$) | 3335 | 13,334 | 30,664 | 3598 | 9784 | 23,008 |
| $A_{lim}$ (Å$^2$) | 2585 | 7908 | 18,690 | 2774 | 5981 | 11,567 |

$A_1$, $A_2$, and $\pi_1$, $\pi_2$, respectively, represent the onset and end areas and pressures of the transition region, which are located at the intersections of the extrapolating lines (prior, in, and beyond the transition region); $A_{on}$ represents the onset molecular area at which obvious surface pressure increase is observed; $A_{lim}$ is determined by extrapolating the linear region of $\pi = 4$–$12$ mN/m to the surface pressure of zero.

$CHCl_3$ and $CCl_4$, while the isotherms of SVP11 monolayer show the featureless lines and the surface pressures rise steeply without transition region. Some important isotherm parameters $A_1$, $A_2$, $\pi_1$, $\pi_2$, $A_{on}$, and $A_{lim}$ for the three samples are listed in Table 2. The parameters $A_1$, $A_2$, and $\pi_1$, $\pi_2$, respectively, represent the onset and end areas and pressures of the transition region, which are located at the intersections of the extrapolating lines (prior, in, and beyond the transition region); $A_{on}$ represents the onset molecular area at which obvious surface pressure increase is observed; $A_{lim}$ is determined by extrapolating the linear region of $\pi = 4$–$12$ mN/m to the surface pressure of zero. According to Table 2, the transition regions ($A_1 - A_2$) of SVP59 are larger than those of SVP28 spread with the corresponding solvents, and the transition regions of the same sample spread with $CHCl_3$ are larger than those spread with $CCl_4$. The larger transition region means that the surface-adsorbed P2VP blocks occupying much larger area are submerged into water. On the other hand, with the increase of P2VP block length, the isotherms (no matter the monolayers spread with $CHCl_3$ or $CCl_4$) move to the larger molecular areas. It is no doubt that the surface-adsorbed P2VP block mainly contributes to the molecular area in the expansion region, and the longer the P2VP block, the larger the area occupied by the surface-adsorbed P2VP blocks. According to the data of $A_{on}$ and $A_{lim}$ listed in Table 2, the same trend can also be drawn.

Since $CCl_4$ is selective for PS, the cores and coronas of the solution micelles were composed of P2VP and PS blocks, respectively. Because of the strong attraction, P2VP blocks tended to spread on the water surface when the solution micelles came into contact with the water. At the same time, PS blocks tended to leave the water surface because they were incompatible with water and P2VP blocks. However, the aggregates retained from the spreading solution would hinder the stretch (or movement) of P2VP blocks on the water surface. Therefore, there are less surface-adsorbed P2VP blocks of SVP28 and SVP59 monolayers spread with $CCl_4$ than those spread with $CHCl_3$. Moreover, it is worthy to note that the

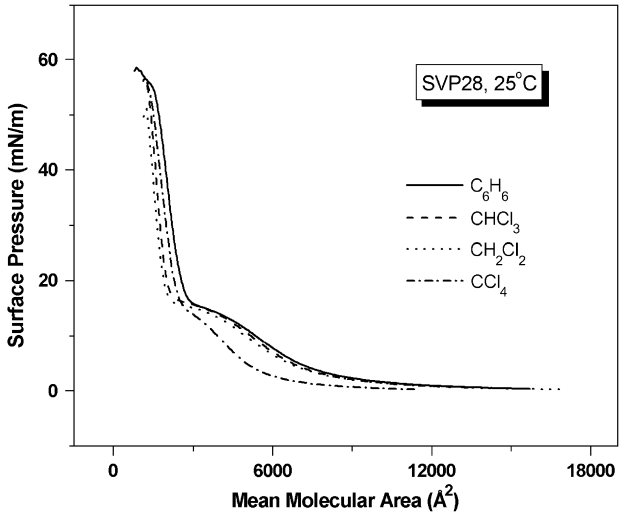


Fig. 2. $\pi$–$A$ isotherms of SVP28 monolayers spread with different solvents at 25 °C.

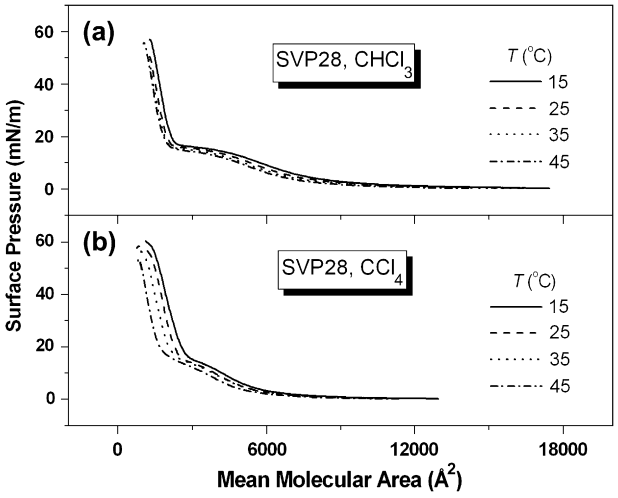


Fig. 3. Temperature effect on the isotherms of SVP28 monolayers spread with $CHCl_3$ (a) and $CCl_4$ (b).

molecular areas of the isotherm of SVP11 spread with $CCl_4$ are larger than those spread with $CHCl_3$, which maybe due to the monolayer spread with $CCl_4$ has formed a less compressible structure (will be mentioned later).

### 3.3. Solvent effect on isotherms

In order to further study the effect of the spreading solvents, the isotherms of SVP28 monolayers spread with three kinds of nonselective solvents are compared with that spread with $CCl_4$ (selective solvent). Fig. 2 shows the $\pi$–$A$ isotherms of SVP28 monolayers spread with nonselective and selective solvents at 25 °C. From Fig. 2, it can be seen that the isotherms of the monolayers spread with the nonselective solvents almost overlap especially in the expansion and the plateau transition regions, which is much different from that spread with $CCl_4$. That is to say, the stretching degrees of P2VP blocks in the monolayers spread with the nonselective solvents are almost the same (stretch completely), while that with the selective solvent is different (stretch incompletely).

### 3.4. Temperature effect on isotherms

Fig. 3 shows the temperature effect on the isotherms of SVP28 monolayers spread with $CHCl_3$ (a) and $CCl_4$ (b). Usually, the temperature dependence of both the plateau pressure and the $A_2$ value is believed to reflect the temperature dependence of the solubilization process [17]. From Fig. 3, it can be seen that the temperature dependence of both the plateau pressure and the $A_2$ value is very small in the two cases (especially in panel a). However, still it can be distinguished that at lower temperatures (i.e. 15 °C) the P2VP block solubilization process is less favorable and the plateau pressure is larger, which is consistent with the greater energy required to solubilize the P2VP block. The whole isotherms (in Fig. 3a) for 35 °C and 45 °C are superposed, which can be contributed to the evolution of the starfish micelles into the complete jellyfish micelles. Moreover, the $A_2$ values in the isotherms of SVP28 monolayers spread with $CCl_4$ (in panel b) significantly move to the small areas with the increase of temperature. At higher temperatures (i.e. 45 °C), both the stretch and solubilization of P2VP blocks are favorable and the P2VP blocks do less contribution to the surface pressure in the solid region.

### 3.5. Hysteresis measurements

Fig. 4a and b show the compression–expansion curves of SVP28 monolayers spread with $CHCl_3$ and $CCl_4$, respectively, at 25 °C. From Fig. 4, it can be seen that there is no hysteresis when the maximum pressure is below the transition plateau. When the maximum pressure reaches or is above the plateau, hysteresis is observed, and the higher the maximum pressure, the larger the hysteresis is. This effect is a good indication that the highly compressed film has undergone some rearrangement process whose kinetic barrier to return to the initial state

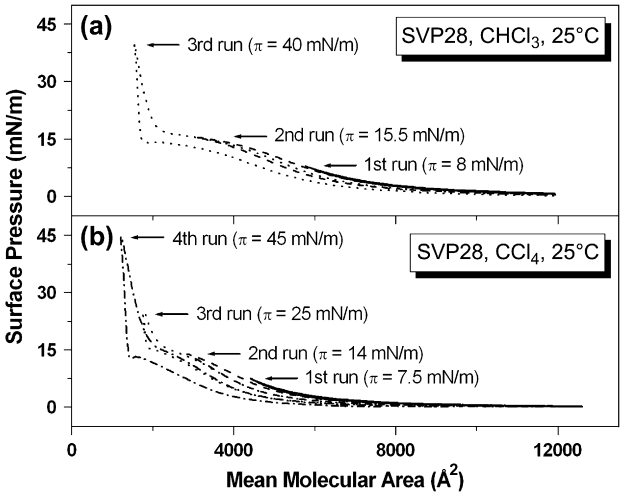


Fig. 4. Compression–expansion curves of SVP28 monolayers spread with $CHCl_3$ (a) and $CCl_4$ (b) at 25 °C.

conformation is rather large [17]. Moreover, it is notable that the compression isotherms (in Fig. 4b) seemed to superpose on the expansion isotherms of the prior cycles. Combined with the morphologies of the corresponding LB films (shown in the following section), that is to say, the compression–expansion process is more irreversible for SVP28 monolayer spread with $CCl_4$ (rodlike structure or labyrinth pattern) than that spread with $CHCl_3$ (isolated circular micelles).

### 3.6. AFM images

Besides of the isotherm data, detailed insight into the organization and morphology of the Langmuir monolayers should rely on the images of their corresponding LB films. We assume that a distortionless transfer has occurred during the deposition of the LB film. In this part, we will compare the morphologies of the three samples deposited at different pressures. Fig. 5

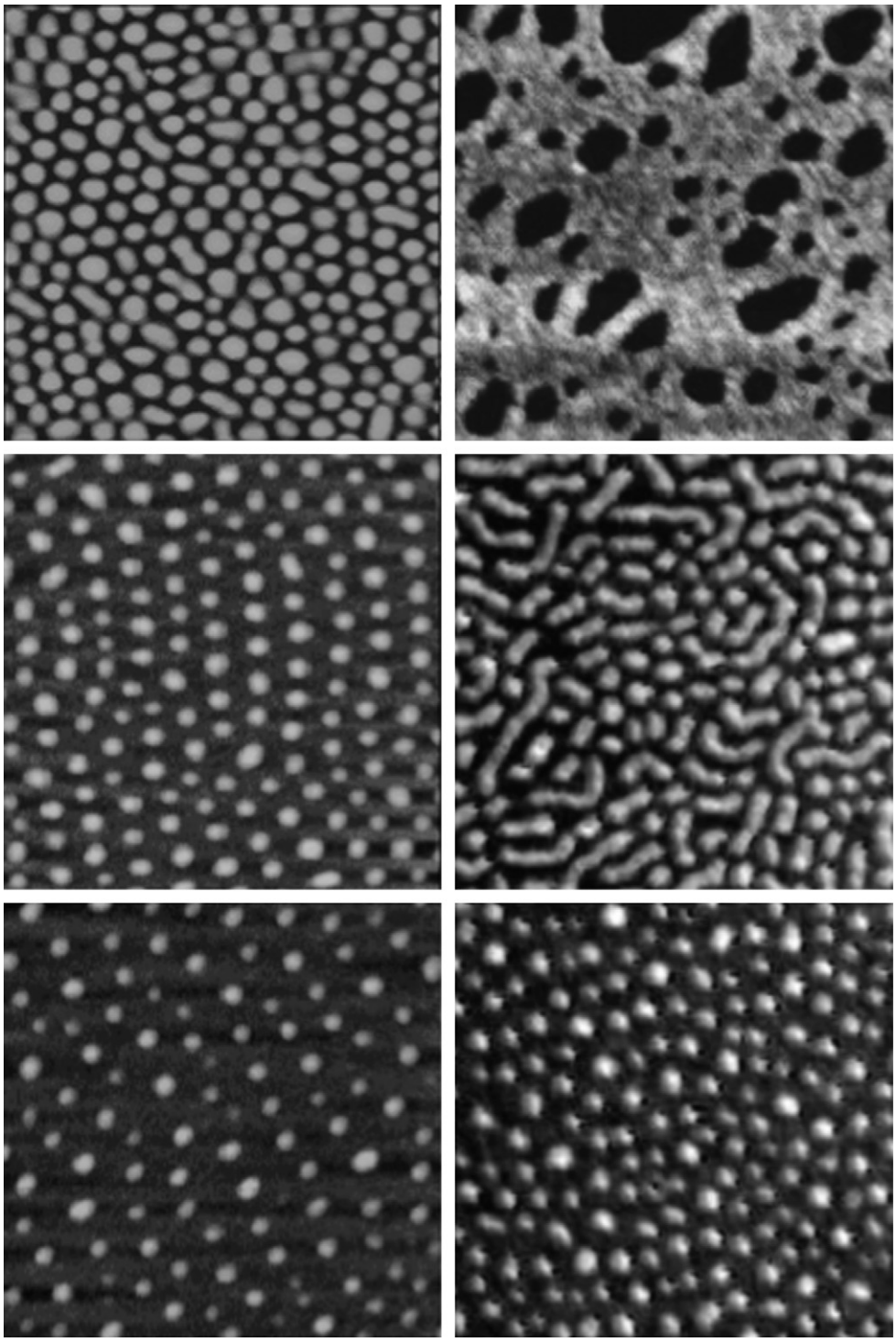

Fig. 5. AFM height images (1 μm × 1 μm) of the LB films of SVP11 (top), SVP28 (middle), and SVP59 (bottom) deposited at 2 mN/m and 25 °C. The spreading solvents are $CHCl_3$ (left) and $CCl_4$ (right). The $Z$ ranges are 3 nm (left), 4 nm (right top), and 8 nm (right middle and bottom).

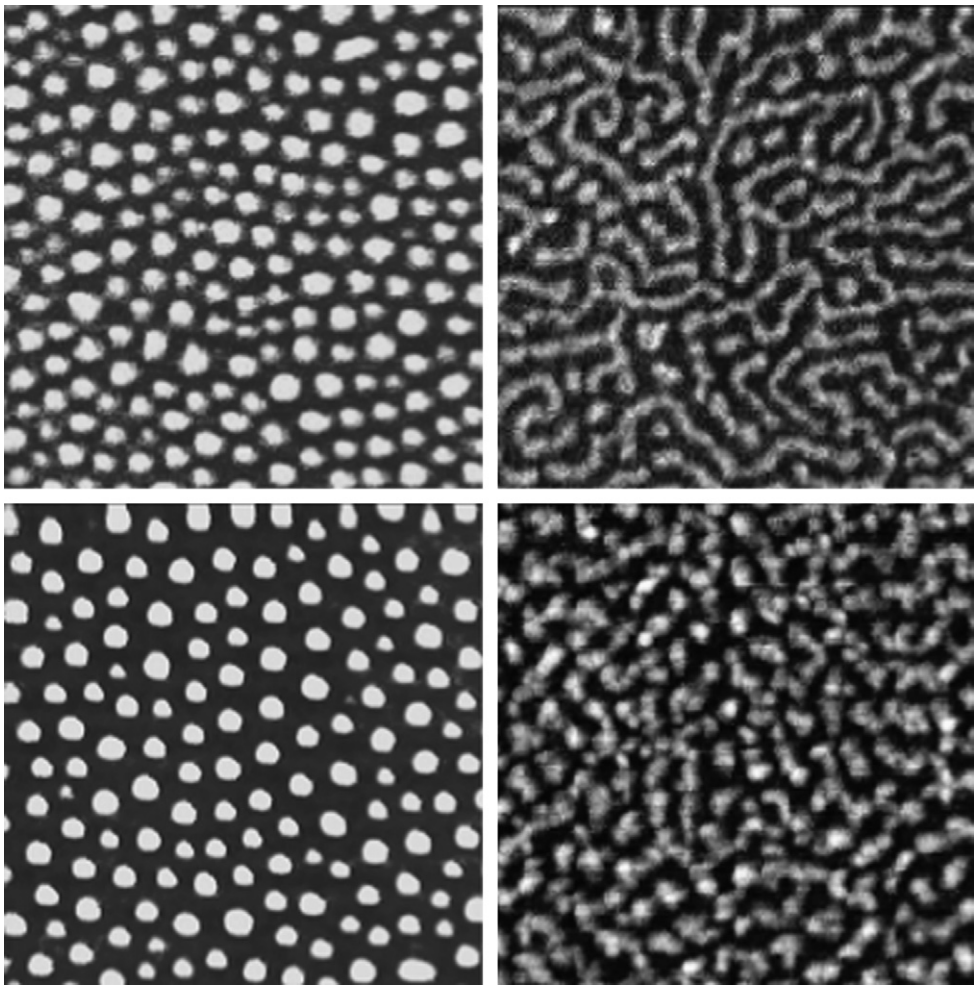

Fig. 6. AFM height images (1 μm × 1 μm) of the LB films of SVP28 (top) and SVP59 (bottom) deposited at 7.5 mN/m and 25 °C. The spreading solvents are $CHCl_3$ (left) and $CCl_4$ (right). The *Z* ranges are 8 nm (left top), 6 nm (left bottom), and 10 nm (right top and bottom).

shows the AFM height images of the LB films of SVP11 (top), SVP28 (middle), and SVP59 (bottom) deposited at 2 mN/m and 25 °C. The spreading solvents are $CHCl_3$ (left) and $CCl_4$ (right). From Fig. 5, it can be seen that all the images of the samples spread with $CHCl_3$ exhibit regular isolated circular micelles and the distances of the cores increase with the increase of P2VP block length. However, the LB films of the samples spread with $CCl_4$ exhibit quite different morphologies, i.e., with the increase of P2VP block length, the morphologies are planar structure with some defects (SVP11) (which is quite different from the polydisperse array of very large planar circular structures [16,17] or planar aggregates with very sharp and straight cracks [35]), mixed morphology of short rods and circular micelles (SVP28), and condensed circular micelles (SVP59). For the samples SVP11 and SVP28, the stretching degrees of P2VP blocks (in the monolayers spread with $CCl_4$) decreased and could not prevent PS cores from further fusing into the planar or short rod structures, respectively. As for the sample SVP59, the stretching degree of P2VP blocks also decreased (the surface micelles with a higher density) but they were still long enough to prevent PS cores from fusing. The planar structure of SVP11 spread with $CCl_4$ is less compressible than the circular structure spread with $CHCl_3$, which is consistent with the isotherms shown in Fig. 1 (molecular areas of the isotherm of SVP11 spread with $CCl_4$ are larger than those spread with $CHCl_3$).

Fig. 6 shows the AFM height images of the LB films of SVP28 (top) and SVP59 (bottom) deposited at 7.5 mN/m and 25 °C. The spreading solvents are $CHCl_3$ (left) and $CCl_4$ (right). From Fig. 6, it can be seen that the images of the two samples spread with $CHCl_3$ still exhibit isolated circular micelles but with higher densities and larger sizes compared with those deposited at 2 mN/m (in Fig. 5). When the monolayers were spread with $CCl_4$, the images of the LB films of SVP28 and SVP59, respectively, exhibit labyrinth pattern (which is quite different from the rodlike aggregates [16,17] or spaghetti structure [35]) and short rod structure (or looks just like PS cores in close). That is, with the further compression (up to 7.5 mN/m) of the monolayers, short rods and circular micelles (at 2 mN/m) in the SVP28 monolayer come in close and tend to form labyrinth pattern (instead of long rod structure, which means they can coalesce stochastically), and the PS cores of the condensed circular micelles (at 2 mN/m) in the SVP59 monolayer come in close and tend to fuse into short rod structure (or just come in close).

Table 3
Aggregation numbers ($N_{agg}$) of the circular micelles for the samples

| Sample | Spreading solvent | Deposition pressure (mN/m) | Number of micelles (μm$^2$) | Molecular area (Å$^2$) | Aggregation number ($N_{agg}$) |
|---|---|---|---|---|---|
| SVP11 | $CHCl_3$ | 2 | 232 | 2691 | 160 |
| SVP28 | $CHCl_3$ | 2 | 154 | 9021 | 72 |
| SVP59 | $CHCl_3$ | 2 | 103 | 22555 | 43 |
| SVP59 | $CCl_4$ | 2 | 174 | 13592 | 42 |
| SVP28 | $CHCl_3$ | 7.5 | 198 | 5850 | 86 |
| SVP59 | $CHCl_3$ | 7.5 | 147 | 14013 | 49 |

As for the sample SVP11 (spread with $CCl_4$), the transfer ratio was zero at the deposition pressure of 7.5 mN/m and failed to prepare the LB film, which maybe due to the rigidity of the monolayer. In the planar structure (at 2 mN/m), we assume the surface-adsorbed short P2VP blocks are underneath the planar or radially extended along the edge of the defects, and the flat surface-adsorbed P2VP blocks can provide enough energy for the deposition of the LB film. However, with the further compression (up to 7.5 mN/m) of the monolayer, smaller and less defects will exist (and the monolayer becomes a little more rigid) and most of the P2VP blocks extended in the defects will solubilize into water, and the limited flat surface-adsorbed P2VP blocks cannot provide enough energy to transfer the relatively rigid monolayer onto the silicon wafer.

The average aggregation numbers ($N_{agg}$) of the circular micelles visualized in Figs. 5 and 6 were calculated with the total area method [14] and shown in Table 3. According to an AFM height image, we counted the number of the micelles and calculated the area per micelle. From the isotherm (in Fig. 1), we knew the molecular area at the corresponding deposition pressure. The area per micelle divided by the molecular area gave the number of molecules per micelle ($N_{agg}$). From Table 3, it can be seen that the $N_{agg}$ decreases with the increase of P2VP block length at a certain deposition pressure, which is due to the stronger repulsive interactions between the longer P2VP blocks. As we know, in the expanded region, the surface pressure mainly contributes to the repulsion of the surface-adsorbed P2VP block, the longer P2VP blocks will occupy larger area and fewer P2VP blocks are needed to provide the repulsion. Moreover, the $N_{agg}$ for the corresponding sample tends to increase with the increase of the deposition pressure, which is easy to understand that the further compression will provide enough energy to overcome some repulsion between the P2VP blocks and form larger aggregates.

## 4. Conclusions

Nonselective and selective solvents were used to spread the diblock copolymers of PS-*b*-P2VP with different P2VP block lengths. The spreading solvents showed large effect on the $\pi$–$A$ isotherms and on the morphologies of the corresponding LB films. The LB films deposited with a nonselective spreading solvent only exhibited isolated circular micelles, while those deposited with a selective spreading solvent exhibited quite different morphologies including planar structure, rodlike structure, circular micelles, and labyrinth pattern. As far as we know, the labyrinth pattern appears in the LB films for the first time. In our opinion, the attraction between water and P2VP block, the repulsion of PS block from both water and P2VP block, together with the stretching degree of P2VP block, can be used to interpret the isotherms and the AFM images.

## Acknowledgments

This work was supported by grants from KOSEF (Center for Integrated Molecular Systems) and the BK 21 program.

## References

[1] Weiser MS, Thomann Y, Heinz LC, Pasch H, Mülhaupt R. Polymer 2006;47:4505.
[2] Ulbricht M. Polymer 2006;47:2217.
[3] Vasilev C, Reiter G, Pispas S, Hadjichristidis N. Polymer 2006;47:330.
[4] Zhu J, Yu H, Jiang W. Polymer 2005;46:11962.
[5] Ho RM, Tseng WH, Fan HW, Chiang YW, Lin CC, Ko BT, et al. Polymer 2005;46:9362.
[6] Lambreva DM, Opitz R, Reiter G, Frederik PM, de Jeu WH. Polymer 2005;46:4868.
[7] Tokarczyk KK, Grumelard J, Haefele T, Meier W. Polymer 2005;46:3540.
[8] Kwee T, Mauritz KA, Beyer FL. Polymer 2005;46:3871.
[9] Costa AC, Chiche A, Vlček P, Creton C, Composto RJ. Polymer 2004;45:4445.
[10] Blackwell RI, Mauritz KA. Polymer 2004;45:3457.
[11] Mauritz KA, Blackwell RI, Beyer FL. Polymer 2004;45:3001.
[12] Minich EA, Nowak AP, Deming TJ, Pochan DJ. Polymer 2004;45:1951.
[13] Zhu J, Eisenberg A, Lennox RB. J Am Chem Soc 1991;113:5583.
[14] Zhu J, Lennox RB, Eisenberg A. Langmuir 1991;7:1579.
[15] Zhu J, Eisenberg A, Lennox RB. Makromol Chem 1992;53:211.
[16] Zhu J, Lennox RB, Eisenberg A. J Phys Chem 1992;96:4727.
[17] Zhu J, Eisenberg A, Lennox RB. Macromolecules 1992;25:6547, 6556.
[18] Li S, Hanley S, Khan I, Varshney SK, Eisenberg A, Lennox RB. Langmuir 1993;9:2243.
[19] Cox JK, Yu K, Constantine B, Eisenberg A, Lennox RB. Langmuir 1999;15:7714.
[20] Bronich TK, Popov AM, Eisenberg A, Kabanov VA, Kabanov AV. Langmuir 2000;16:481.
[21] Lin B, Rice SA, Weitz DA. J Chem Phys 1993;99:8308.
[22] Simoes Gamboa AL, Filipe EJM, Brogueira P. Nano Lett 2002;2:1083.
[23] Francis R, Skolnik AM, Carino SR, Logan JL, Underhill RS, Angot S, et al. Macromolecules 2002;35:6483.
[24] Kumaki J, Hashimoto T. J Am Chem Soc 2003;125:4907.
[25] Ahmed F, Hategan A, Discher DE, Discher BM. Langmuir 2003;19:6505.
[26] Cheyne RB, Moffitt MG. Langmuir 2005;21:5453.
[27] Logan JL, Masse P, Dorvel B, Skolnik AM, Sheiko SS, Francis R, et al. Langmuir 2005;21:3424.
[28] An SW, Su TJ, Tomas RK, Baines FL, Billingham NC, Armes SP, et al. J Phys Chem B 1998;102:387.
[29] Israechvili J. Langmuir 1994;10:3774.
[30] Goncalves da Silva AM, Simoes Gamboa AL, Martinho JMG. Langmuir 1998;14:5327.
[31] Ferreira M, Constantino CJL, Olivati CA, Balogh DT, Aroca RF, Faria RM, et al. Polymer 2005;46:5140.
[32] Chung B, Choi M, Ree M, Jung JC, Zin WC, Chang T. Macromolecules 2006;39:684.
[33] Chung B, Park S, Chang T. Macromolecules 2005;38:6122.
[34] Baker SM, Leach KA, Devereaux CE, Gragson DE. Macromolecules 2000;33:5432.

[35] Devereaux CA, Baker SM. Macromolecules 2002;35:1921.
[36] Sohn B, Yoo S, Seo B, Yun S, Park S. J Am Chem Soc 2001;123:12734.
[37] Meiners JC, Quintel-Ritzi A, Mlynek J, Elbs H, Krausch G. Macromolecules 1997;30:4945.
[38] Li Z, Zhao W, Liu Y, Rafailovich MH, Sokolov J, Khougaz K, et al. J Am Chem Soc 1996;118:10892.
[39] Meiners JC, Elbs H, Mlynek J, Krausch G. J Appl Phys 1996;80:2224.
[40] Spatz JP, Sheiko S, Möller M. Macromolecules 1996;29:3220.
[41] Spatz JP, Roescher A, Möller M. Adv Mater 1996;8:337.
[42] Verdonck B, Gohy JF, Khousakoun E, Jérôme R, Prez FD. Polymer 2005; 46:9899.
[43] Riegel IC, Samios D, Petzhold CL, Eisenberg A. Polymer 2003;44:2117.
[44] Lee RS, Li HR, Yang JM, Tsai FY. Polymer 2005;46:10718.
[45] Riegler H, Engel M. Ber Bunsen-Ges Phys Chem 1991;95:1424.